SANDIA REPORT

SAND2016-11070
Unlimited Release
Printed October 2016

A model for grain growth during welding

John A. Mitchell, Veena Tikare

Prepared by
Sandia National Laboratories
Albuquerque, New Mexico 87185 and Livermore, California 94550

Sandia National Laboratories is a multi-mission laboratory managed and operated by Sandia Corporation, a wholly owned subsidiary of Lockheed Martin Corporation, for the U.S. Department of Energy's National Nuclear Security Administration under contract DE-AC04-94AL85000.

Sandia National Laboratories

Issued by Sandia National Laboratories, operated for the United States Department of Energy by Sandia Corporation.

Available to DOE and DOE contractors from
U.S. Department of Energy
Office of Scientific and Technical Information
P.O. Box 62
Oak Ridge, TN 37831

Telephone: (865) 576-8401
Facsimile: (865) 576-5728
E-Mail: reports@adonis.osti.gov
Online ordering: http://www.osti.gov/bridge

Available to the public from
U.S. Department of Commerce
National Technical Information Service
5285 Port Royal Rd
Springfield, VA 22161

Telephone: (800) 553-6847
Facsimile: (703) 605-6900
E-Mail: orders@ntis.fedworld.gov
Online ordering: http://www.ntis.gov/help/ordermethods.asp?loc=7-4-0#online

SAND2016-11070
Unlimited Release
Printed October 2016

A model for grain growth during welding

John A. Mitchell and Veena Tikare
Multiscale Science

Sandia National Laboratories
1515 Eubank SE
Albuquerque, NM 87185

Abstract

This report describes and demonstrates a new model for grain growth during welding of metals. The model is implemented in the SPPARKS C++ kinetic Monte Carlo computational framework and can run large scale, massively parallel simulations using billions of sites. The model simulates melting, solidification and microstructural evolution of material in the fusion and heat affected zones; it simulates grain growth using normal curvature driven grain growth with grain boundary mobility that is dependent upon a spatial temperature profile. The model is parameterized to facilitate weld design via weld speed and shape parameters for the pool and heat affected zone. Weld speed is a key process parameter and shape parameters describe a wide range of possible pool shapes and heat affected zones facilitating design of many possible weld processes including both convex and concave weld pool shapes. Pool shapes can range from very narrow and deep to very wide and shallow representing different fluid flow conditions within the pool. The model also includes a novel and specialized pulsed power welding feature. Demonstration calculations depict grain growth which is spatially heterogeneous including epitaxial grain growth.

Acknowledgment

The authors wish to express appreciation to the following individuals whose support made this work possible: Jim Redmond (ASC P&EM), Anthony Geller (ASC P&EM Advanced Manufacturing), Daniel Clayton and Chris Jones (Radioisotope Power System Launch Safety). Special thanks to Steve Plimpton for help and advise on SPPARKS implementation details. Discussions on pulse welding with Charlie Robino are also noted and appreciated.

Contents

1 Introduction 9
2 Model for grain growth during welding 11
2.1 Grain growth, melting and solidification 12
3 Temperature profile and its motion 14
3.1 Geometry of weld pool and heat affected zone 14
3.2 Numerical computations for translating weld pool and heat affected zone 15
3.3 Scaling pool geometry to model pulsed power welding 17
4 Application of model 21
4.1 Qualitative predictions and trends 21
5 Summary and conclusions 30
References 33

List of Figures

1 Butt weld schematic. 11
2 Weld schematic. 12
3 Schematic of surrogate weld pool geometry and coordinate system. 15
4 Sketch of closest point projection for calculation of distance to pool surface. . 16
5 Example 3D pool geometry rendered from 3 different view points. 18
6 Schematic of pool geometry parameters and affects. 19
7 Pulsed weld schematic and concept. 20
8 Depiction of types of grain growth predicted by model 22
9 Weld speed study – top view of predicted microstructures 25
10 Weld speed study – transverse section view of predicted microstructures 26
11 Weld speed study – longitudinal section view of predicted microstructures. . . 26
12 Convexity and concavity study: top view of predicted microstructures. 27
13 Convexity and concavity study: transverse cut of predicted microstructures. . 27
14 Convexity and concavity study: longitudinal cut of predicted microstructures. 27
15 Size and shape study: top view of predicted microstructures. 28
16 Size and shape study: transverse cut of predicted microstructures. 28
17 Size and shape study: longitudinal cut of predicted microstructures. 28
18 Pulsed power weld speed study – top view of predicted microstructures. 29

List of Tables

1 Model parameters: size, shape, weld speed and pulsed power. 17
2 Model parameters for weld speed study. 23

1 Introduction

Welding is one of the most commonly used processes for joining metals and the resulting joints physical properties are central to the engineering performance of that technology. Welding consists of applying heat to a localized region of two parts which are to be joined; heat melts the region in contact so that the parts fuse to form a single strongly bonded part when cooled and solidified. The heat source is moved along the length of the two parts, so that the molten pool is leading and the cooling and solidifying welded region is trailing. This moving heat source leads to the unique microstructures observed in welds, characterized by elongated grains that can curve in different directions to give banana-shaped grains. The size and shape of grains in the weld influence mechanical and other engineering properties; thus, it is important to understand and predict weld microstructures as a function of the welding process, so that its engineering properties can be tailored to its performance in service environments. To this end, we present a model that can simulate melting and solidification in the fusion zone and grain growth in the fusion and heat-effected zones during the welding process. Such a modeling capability can be used for designing the welding process to obtain microstructures that yield optimal properties.

Solidification, microstructural evolution and fluid flow [1, 2] in the fusion zone of welds have been the topic of many investigations [3]. Modeling of solidification during welding has focused primarily on dendritic growth at the solid-liquid interface in thermal gradients [4, 5, 6, 7, 8, 9, 10]; others focus on the coupling between heat and/or fluid flow and grain growth [11] or grain shape characteristics in limited regions [12, 13, 14]. These works have provided much understanding of the details of solidification; however, by their nature to treat details of solidification, they are limited to small regions of a few grains. Recently, a few have addressed grain growth on a larger scale in the welding region. Chen et al. [15] developed a coupled cellular automaton and finite element model to calculate the temperature profile in welding region using FE modeling and grain growth in the fusion zone. While, this does give information of many hundreds of grains, it does not consider the grain growth in the heat-affected zone, which we will show influences microstructure greatly. Debroy and coworkers [16, 17, 18] developed models to simulate grain growth in the heat affected zone (HAZ), but not the fusion zone (FZ). This, unfortunately, does not yield microstructural information for the most pertinent portion of the weld. The method we present has many similarities to the work of Zacharia and coworkers [19, 20]; however, they limited their grain growth simulations to 2D simulations (using cellular automata) at the surface of the weld zone.

The Potts Monte Carlo model, described in previous works [21, 22], has been modified to simulate grain growth during welding. Grain growth with non-uniform grain boundary mobility due to large gradients in temperature are incorporated in the model as described previously [23]. A new algorithm is introduced that incorporates melting and solidification of the melt pool accompanying welding. This model to simulate grain growth during welding is an application in SPPARKS [24], an open-source Sandia code developed for simulation of microstructural evolution using Monte Carlo methods. Due to the novel treatment of pool geometry and heat affected zone, the model can be used to simulate pulsed power welding in which power is cycled between a lower background level and a maximum level. The welding

model uses key process parameters as inputs to simulate grain growth during welding; it can be used in parallel with experiments to guide selection of weld process parameters in order to achieve a desired microstructure. A related weld model [25], targeting electron beam welding, was recently published by co-workers using identical temperature dependent grain growth kinetics but different treatment and handling of pool geometry; the model by Rodgers et. al. does not include the effects of pulsed welding nor does it handle pool geometry as mathematically precisely as does the present work. This report presents the newer model and demonstrates it utility for use in weld process design and prediction of trends in microstructure due to systematic changes in process parameters. The model is available via the SPPARKS website [26].

2 Model for grain growth during welding

A schematic, shown in Figure 1, depicts the butt-welding process. Two sheets of material, with the same thickness, are just touching (butt-joint). Heat is applied to the upper surfaces of the sheets along the line formed by the edges of the two plates. As the heat source moves along the butt-joint, a molten pool of metal that penetrates the full thickness of both plates forms and then solidifies to join the two sheets in the butt-weld. Surrounding the molten fusion zone (FZ), is the heat-affected zone (HAZ), where the temperature is high, but below the melting temperature; a depiction is shown in Figure 2. Material in the near vicinity of the weld pool, i.e. in the HAZ, experiences a transient rise and fall of temperature which induces microstructure evolution. As the heat source moves away the butt-joint material and the HAZ cool and a complex grain structure forms. Engineering properties such as strength and toughness critically depend upon this microstructure. We present a model that simulates melting under the heat source, with solidification and grain growth in the HAZ. This section describes the model for grain growth during welding; it is based on the Potts grain growth model.

Note, the Potts model as described in this work, requires a temperature as a function of position and time. Based on this, it simulates melting as occurring in regions where the temperature exceeds the melting temperature and solidification as occurring in the region where the temperature drops below the melting temperature. Grain growth is simulated by the normal curvature-driven grain growth model, but the grain boundary mobility is a function of temperature. Details of solidification, such as dendritic growth, are not treated by this model. It also does not simulate fluid motion in the molten pool or heat transfer elsewhere; however, these elements are and can be implicitly included via the spatial and temporal temperature profile input to this model.

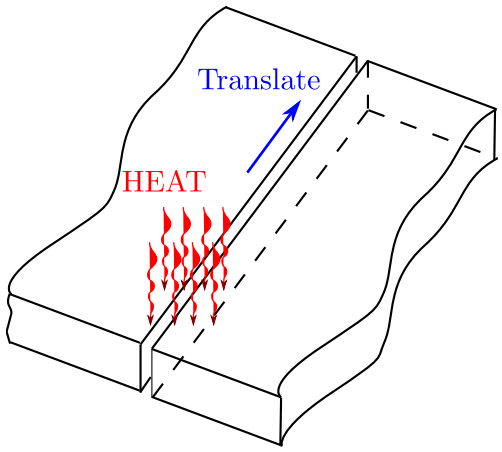

Figure 1: Butt weld schematic. Weld heat is applied and translated along butt joint formed by two plates of same thickness that are just touching. Separation of plates shown for clarity.

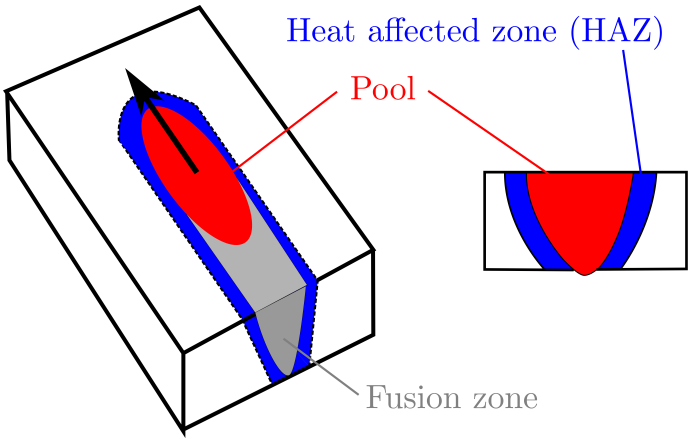

Figure 2: Weld schematic.

2.1 Grain growth, melting and solidification

The standard Potts model for grain growth digitizes the 3D microstructure on a regular lattice with each site identified as belonging to a particular grain with a unique identifier, termed spin. All contiguous sites with the same identifier constitute a grain. The starting microstructure for the welding simulation is the grain structure of the two sheets to be welded. For the purposes of this model, the two sheets are assumed to be in perfect contact; the temperature profile resulting from the moving heat source is applied to the initial microstructure.

The equation of state used for grain growth simulations only considers grain boundary energy, as the reduction in grain boundary energy is the driving force for grain growth. The total energy of the system is the total grain boundary energy, which is calculated as the sum of all bonds between neighboring sites with dissimilar spins multiplied by the bond energy as

$$E = \frac{J}{2} \sum_{i}^{N} \sum_{j}^{n} (1 - \delta_{ij}), \tag{1}$$

where J is the bond energy, i is each site ranging from 1 to the total number of sites, N, j is the neighbor of site i ranging from 1 to n, and n is the number of neighbors of i. Thus, grain boundaries are identified in this model as occurring between neighboring sites of dissimilar spins with an associated bond energy between them of J.

Curvature-driven grain growth is simulated by selecting a site and attempting to change its spin, its grain identifier, to that of a neighboring site belonging to a different grain. Interior sites with no neighboring sites belonging to a different grain cannot change their spin (because it is energetically unfavorable), only grain boundary sites can. When a site attempts to change it spin, if it has no neighboring sites of a different spin, then the attempt is not successful and another site attempts a change. When a grain boundary site attempts to change its spin, it selects a spin from one of its neighboring grains at random. The change

in energy accompanying this spin flip is calculated using (1). The probability P of that change occurring is

$$P = \begin{cases} 1 & \Delta E \leq 0 \\ e^{-\frac{\Delta E}{kT}} & \Delta E > 0. \end{cases} \tag{2}$$

The attempted change in spin is always successful when $\Delta E \leq 0$ and when $\Delta E > 0$, it occurs in proportion to the probability (2) using the Metropolis algorithm. A random number, R evenly distributed from 0 to 1 is generated. If $R \leq P$, the attempted change is successful, if not the original spin remains. The product kT has units of energy, and in the context here, kT is referred to as the simulation temperature and is a SPPARKS model parameter.

Previous work has shown how temperature-dependent grain growth can be simulated by introducing a grain boundary mobility term that is a function of temperature, $M(T)$, where T is the physical temperature during welding.

$$P = \begin{cases} M(T) & \Delta E \leq 0 \\ M(T)e^{-\frac{\Delta E}{kT}} & \Delta E > 0. \end{cases} \tag{3}$$

The grain boundary mobility increases with temperature until the melting temperature, when grain boundaries cease to exist in the molten region. At ambient temperatures, $M = 0$, as the temperature is too low for grain growth.

Simulation of melting and solidification is introduced into this model as follows. When the temperature at site i is equal or greater than the melting temperature $T \geq T_m$, melting is simulated by assigning a random spin to site i that is likely different from those of its neighboring sites. Thus, the grain structure is lost and the energy of site j is very high as its bonds with all neighboring sites have energy J. When the temperature of site i is less that the melting temperature, $T < T_m$, normal grain growth is attempted with a new spin that is randomly chosen from those of neighboring sites. Thus, when the temperature of a site drops below T_m, it will solidify by changing its spin to that of a neighboring site, lowering its energy and forming a grain of at least two sites. In this manner, melting and solidification is simulated in this model.

3 Temperature profile and its motion

This section describes details of the grain growth model for butt-welds implemented in SPPARKS. As described in Section 2, the model does not calculate the temperature; rather, the temperature profile, both spatial and temporal, is an input to the grain growth model. Based upon experimental or analytical/numerical calculations, a representative temperature profile, which can be changed to match a physical welding process, is used as an input to the numerical model.

The numerical implementation, described here, uses surrogate analytical temperature profiles for a butt-weld process. A geometric parameterization representing a family of weld pool temperature profiles was used for numerical computations. A schematic of the surrogate weld pool geometry is shown in Figure 3. Key elements of the temperature profile and model are shape of molten weld pool, geometry and shape of the heat affected zone (HAZ), and computing grain boundary mobility M for use in the grain growth model described in earlier in Section 2. The geometry and translation of the weld-pool and HAZ are the backbone of the numerical implementation. Using these temperature profiles, it is shown later in Section 4, that the shape and speed of the weld pool and HAZ strongly influence grain growth and evolution, and the resulting microstructure.

3.1 Geometry of weld pool and heat affected zone

The shape and size of the FZ and HAZ (see Figure 2) are functions of the total heat deposited and its distribution in the plates to be welded, the velocity of heat source along the weld joint, the resulting fluid flow in the molten pool, and solidification details. Using the model presented here, these aspects are bypassed by simply treating the local temperature as an input to the simulation. The geometry of the HAZ is inspired by the idea that the pool surface is nominally at the melt temperature and that temperature proportionally drops with distance from the surface. The pool geometry is represented as a surface separating the liquid melt (inside of pool) from the solid (outside pool). The HAZ is a region outside the pool defined by a model parameter haz representing the distance from the pool surface.

In order to precisely define the HAZ, some notation and semantics describing points inside and outside the weld pool are introduced. Let $\mathbb{D} \subset \mathbb{R}^3$ be the bounded spatial domain representing the plates to be joined by the weld. Let $\mathbb{P}$ denote the set of points inside the weld pool; for clarity, note that $\mathbb{P} \subset \mathbb{D}$. The HAZ is defined as those points in $\mathbb{D}$ that are not part of the pool $\mathbb{P}$ but are are within a distance haz of the pool surface. It is useful to define the set of points $\mathbb{V} = \mathbb{D}/\mathbb{P}$; these are points within the plates but outside of the pool. Using these notations, the heat affected zone is the set of points HAZ defined as

$$\text{HAZ} := \{\mathbf{y} : \mathbf{y} \in \mathbb{V} \text{ and } d(\mathbf{y}) \leq haz\}, \tag{4}$$

where $d(\mathbf{x})$ denotes the Euclidean distance to the pool surface for a point $x \in \mathbb{V}$.

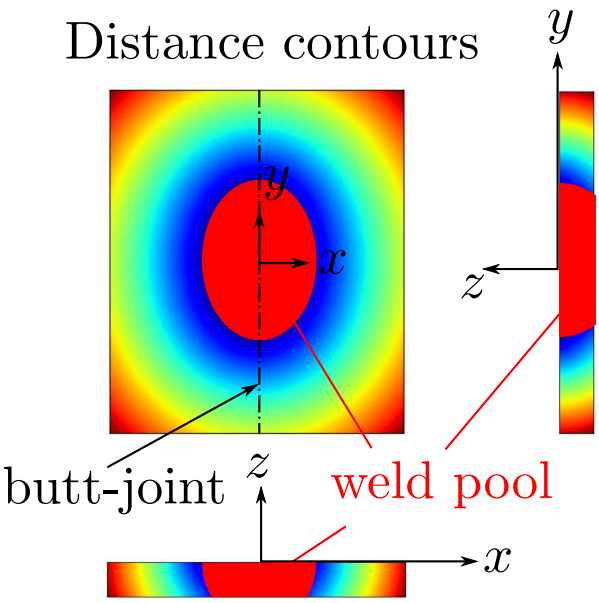

Figure 3: Schematic of surrogate weld pool geometry and coordinate system; distance contours used to define heat affected zone.

The grain boundary mobility (described in Section 2) is now defined as a function of position for points $\mathbf{x} \in$ HAZ:

$$M(\mathbf{x}) = 1 - d(\mathbf{x})/haz. \tag{5}$$

3.2 Numerical computations for translating weld pool and heat affected zone

As described above, the idealized weld process consists of translating a source of heat (and hence weld pool) along the butt-joint (see Figures 1 and 2). In this section, numerical computations used to calculate the instantaneous HAZ around the weld pool are outlined and described.

The weld pool is translated along the butt-joint with a constant velocity $\mathbf{v}_p$. With respect to a fixed global coordinate system, the position of the translating coordinate system depicted in Figure 3, is

$$\mathbf{y}_p(t) = \mathbf{y}_p(0) + \mathbf{v}_p\, t. \tag{6}$$

Abstractly, the pool surface is described by a smooth function of two parametric variables $\rho(u, v)$. For any point $\mathbf{r} \in$ HAZ, measured with respect to the pool coordinate system, the distance $d(\mathbf{r})$ must be computed – this computation is accomplished using a closest point projection (CPP) algorithm [27]; a sketch is shown in Figure 4. To calculate the distance

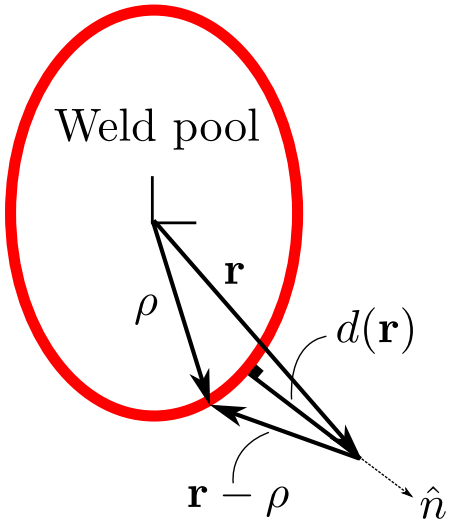

Figure 4: Sketch of closest point projection for calculation of distance to pool surface.

$d(\mathbf{r})$, the CPP algorithm minimizes the square of the distance function

$$f(u,v) = d^2(\mathbf{r}) = (\mathbf{r}-\rho)\cdot(\mathbf{r}-\rho), \tag{7}$$

where for simplicity of notation, the dependence of ρ on the pair of parametric surface variables (u,v) is dropped. Conceptually, the CPP algorithm seeks the point on the pool surface that will form a normal $\hat{n}$ to the surface when connected with the tip of $\mathbf{r}$; this is depicted in Figure 4.

Given a particular form of the analytical pool surface, the CPP algorithm is implemented and the distance is subsequently calculated for any pool position and point. Given the distance to the surface, the mobility (see (5)) for any point outside of the pool can be calculated.

For calculations described in Section 4, the particular geometry used for the surface is briefly described. The pool surface is represented by a quadratic Bézier curve with control points [28] defined by a trigonometric representation of an ellipse. The Bernstein polynomials for the Bézier curve are given by

$$V_0(v) = (1-v)^2, \quad V_1(v) = 2v(1-v), \quad V_2(v) = v^2, \tag{8}$$

with control points defined using the following vector components:

$$P_0(u) = \begin{Bmatrix} x(u) \\ y(u) \\ 0 \end{Bmatrix}, P_1(u) = \begin{Bmatrix} \alpha(1-\beta)x(u) \\ \alpha(1-\beta)y(u) \\ -h/2 \end{Bmatrix}, P_2(u) = \begin{Bmatrix} \alpha x(u) \\ \alpha y(u) \\ -h \end{Bmatrix}. \tag{9}$$

The functions $x(u)$ and $y(u)$ are used to define an ellipse:

$$x(u) = a\cos(u), \quad y(u) = b\sin(u), \tag{10}$$

where the major dimensions of the ellipse are denoted by the parameters (a, b). Using the polynomials in (8) and the control points in (9), the pool surface is defined as

$$\rho(u, v) = V_0(v)P_0(u) + V_1(v)P_1(u) + V_2(v)P_2(u). \tag{11}$$

Note that P_0 corresponds with the top surface at $z = 0$, and that P_1 corresponds with $z = -h$ at the bottom surface; P_1 is associated with the control point and is artificially positioned midway through the thickness of the plate at $z = -h/2$; an additional control of the shape through the thickness is provided by the parameter β to control convexity of the shape related to the thickness dimension. The parameter α determines the size of the ellipse on the bottom surface at $z = -h$; in the calculations for this paper, it is always used in the range $\alpha \in (0, 1)$ to create an ellipse on the bottom which is smaller than the one at the top. All of the size and shape parameters for the weld pool are listed and briefly described in Table 1.

Parameter	**Description**
a	principal dimension ellipse x-axis
b	principal dimension ellipse y-axis
haz	distance parameter representing size of HAZ
h	plate thickness
$\alpha \in (0, 1]$	defines size of ellipse on bottom surface relative to size on top
$\beta \in [0, 1]$	control point parameter; $\beta = 1/2$ produces linear Bézier function
$\mathbf{v}_p$	weld speed expressed in sites per Monte Carlo step (MCS)
$A \in (0, 1)$	defines amplitude of pulsed power oscillations
$N > 2$	defines period of pulse power oscillations in MCS

Table 1: Model parameters: size, shape, weld speed and pulsed power.

The pool surface, defined in (11), is parameterized by $u \in [0, 1]$ and $v \in [0, 2\pi]$; these are the parameters that the CPP algorithm computes for each point in the HAZ. It is emphasized that the pool surface/geometry is a three-dimensional object; an instance is depicted from three different view points in Figure 5. To aid in use and understanding of the parameters α and β, a schematic depicting effects of these parameters on pool geometry in the thickness dimension of the plate is shown in Figure 6.

3.3 Scaling pool geometry to model pulsed power welding

The utility of this model for designing weld processes is demonstrated by applying it to a specialty welding technique, pulsed power welding [personal communication with Charlie Robino, February, 2015]. The concept is depicted in Figure 7; power is cycled between a peak value and a background level at a particular frequency. The interpretation is that higher arc power induces a larger pool while reducing the power will result in a smaller pool; power is supplied in a periodic fashion as a function of time. Emulating this effect in the model is accomplished by defining a pulse function

$$p(t) = B + A\sin(\omega t), \tag{12}$$

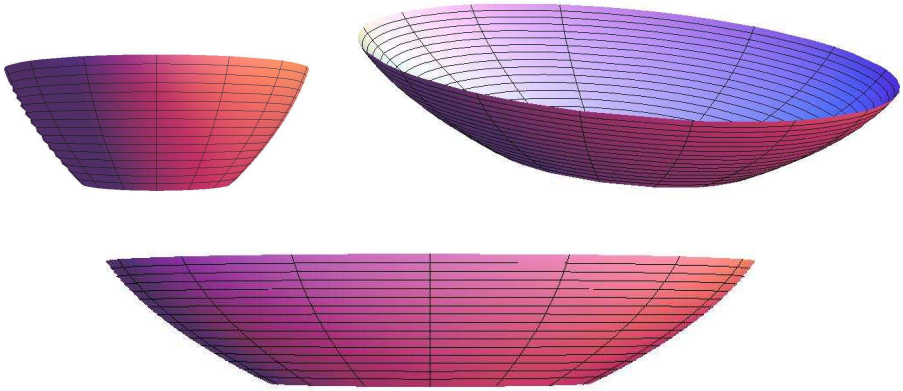

Figure 5: Example 3D pool geometry rendered from 3 different view points.

where $B = 1.0$ denotes a background power representing a nominal pool size, A denotes an amplitude of increase in background power representing an increase in pool size, t is time in MCS, and N is the time period defining the frequency of power oscillations $\omega = \frac{2\pi}{N}$. Using the pulse function (12), the pool geometry (see equations (10)) is scaled and becomes a function of time

$$x(u,t) = p(t)a\cos(u), \quad y(u,t) = p(t)b\sin(u). \tag{13}$$

Pulsed power parameters are also listed in Table 1. The pulse scaling above appears more simple than it is in practice; the above equations are implemented in SPPARKS exactly as described; however, the pulse effect implicitly depends upon the weld speed velocity; demonstration calculations in the sequel illustrate this aspect of the model.

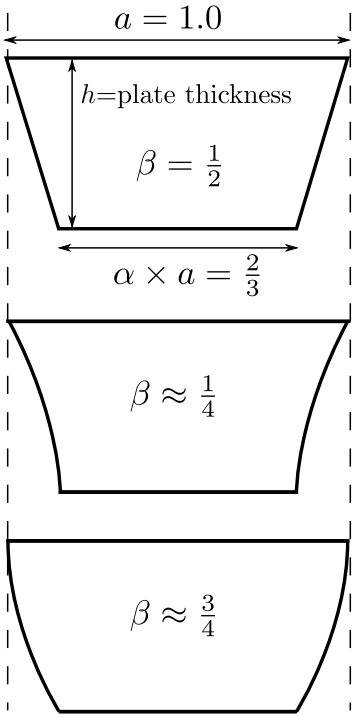

Figure 6: Schematic of pool geometry parameters and affects.

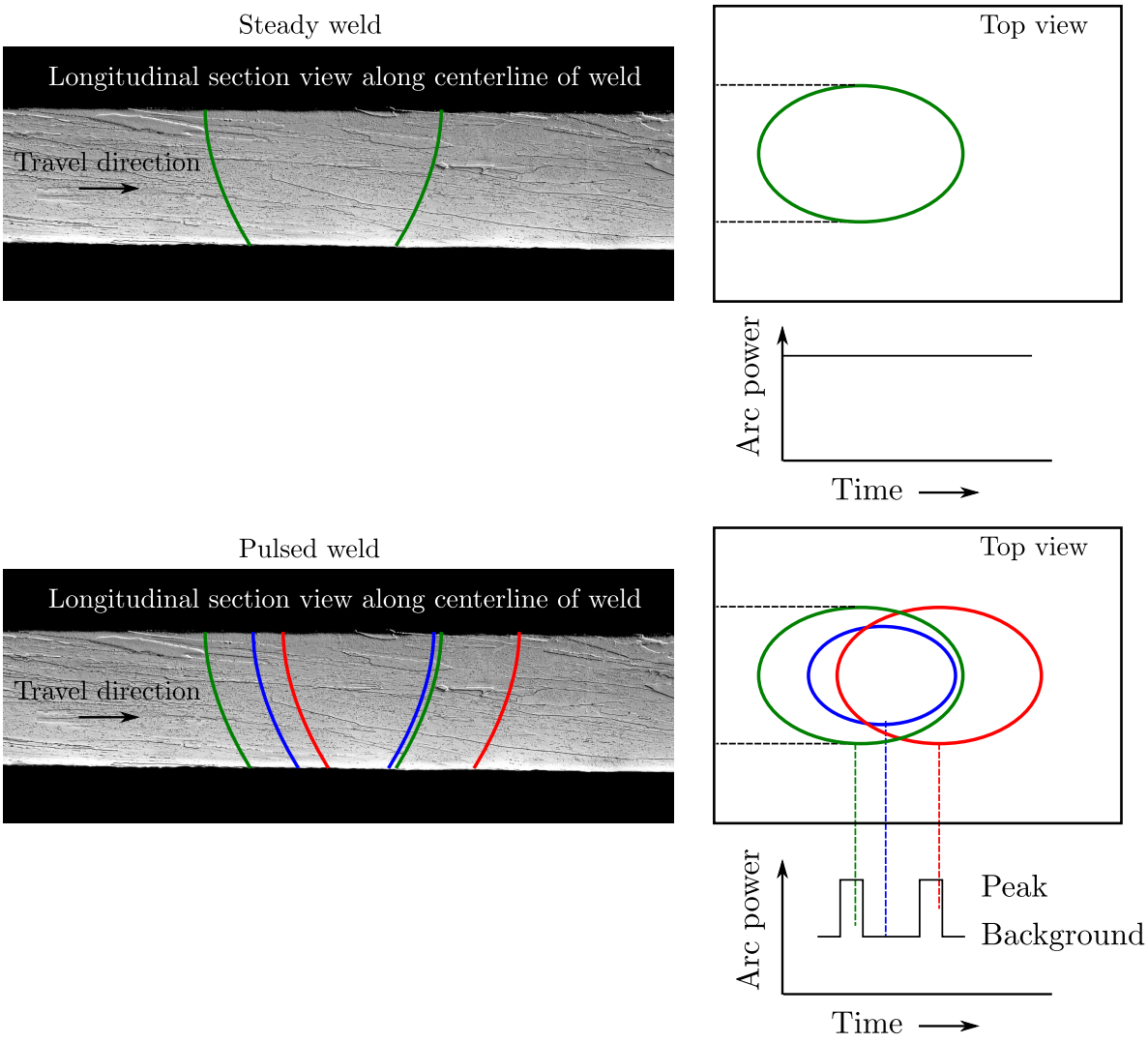

Figure 7: Pulsed weld schematic and concept.

4 Application of model

In this section, the model is used to qualitatively demonstrate grain growth during welding for parametric variations in pool geometry and weld speed. Trends in grain growth patterns are illustrated graphically as a function of weld speed and pool shape; key trends are easily identified and suggest tactics for quantitative analysis. Quantitative analysis is far more challenging and visual inspection of graphical results suggests strategies and methods akin to data analytics; this will be the subject of follow-up work.

4.1 Qualitative predictions and trends

In this section, trends and changes in grain growth and morphology are illustrated as functions of weld pool shape and weld speed. As a starting point, all welding grain growth simulations need an initial microstructure; this was generated using *app_potts_neighonly* in SPPARKS with a simulation temperature of $kT = 0.25$ on a *3D* computational lattice *sc/26n* with dimensions $805 \times 1575 \times 105$; the Potts model will generally produce an equiaxed microstructure dependent upon an initial *seed* value. For the weld speed and pool shape studies in the following sections, a unique initial microstructure was generated for each case using a new random seed value; in all cases, a target mean value for equiaxed grain size was $\mu = 3.6 sites$. Generating initial microstructures with a random seed is especially important when using SPPARKS to generate many microstructure realizations for use in statistical analysis studies.

4.1.1 Types of grain growth

As a prequel to parametric studies, Figure 8 depicts three types of grain growth predicted by the model: nucleation and growth of new grains, epitaxial growth on to existing grains in the HAZ to form long curved grains, and normal grain growth at the outer, cooler regions of the HAZ. Nucleation and growth of new grains occurs in the FZ and is strongly dependent upon weld speed and molten pool geometry. The size and shape of epitaxially grown grains are also strongly dependent on weld speed, molten pool geometry and temperature profile in the HAZ.

4.1.2 Weld speed study

In the first study, weld pool and HAZ shape and size are fixed and the weld speed is incrementally increased from a speed $||\mathbf{v}_p||$ to $2||\mathbf{v}_p||$; see Table 2 for weld speed and shape parameters used.

Predicted microstructures are shown in Figures 9 to 11. Using 4 different weld speeds, these figures illustrate microstructures when viewed from the top, and in transverse and

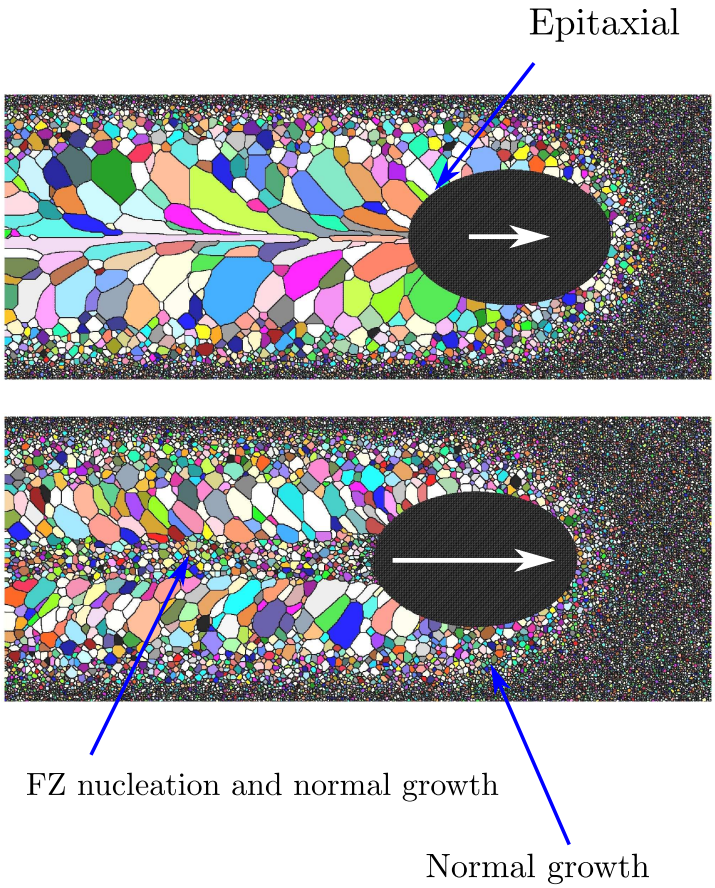

Figure 8: Depiction of types of grain growth predicted by model; weld speed used to generate upper microstructure was half that used to predict lower microstructure.

longitudinal cuts respectively; because these simulations are 3D, transverse and longitudinal cut view images are shown based upon the cut indicators in the top image of Figure 9. The weld pool was translated from left to right with its final position such that the trailing edge was at a distance from the right edge of the image just greater than haz; the bottom image in each figure was generated with twice the weld speed used for the image at the top; the pool shape parameter $\beta = \frac{1}{2}$ was used to produce a linear Bézier curve in the thickness direction of the plate – see Figure 11 for a longitudinal section view of predicted microstructures.

As shown, slower weld speeds encourage epitaxial grain growth, with grains growing normal to the melt pool boundary; as weld speeds increase epitaxial growth diminishes in favor of nucleation and growth of new grains in the center of the FZ.

4.1.3 Weld pool shape study

In the previous section, weld velocity was varied while holding the melt pool and HAZ geometry constant; as shown in Figure 11, the sidewall of the pool had a constant slope through the thickness of the weld. In this section, the melt pool geometry is varied while

Parameter	Value
principal dimension ellipse x-axis	$a = 300$
principal dimension ellipse y-axis	$b = 450$
distance parameter representing size of HAZ	$haz = 150$
plate thickness	$h = 105$
size of ellipse on bottom surface relative to size on top	$\alpha = 0.75$
Bézier control point parameter	$\beta = 0.50$
weld speed	$\|\|\mathbf{v}_p\|\| = \{7.5, 10.0, 12.5, 15.0\}$

Table 2: Model parameters for weld speed study.

holding the weld velocity constant. Two of the four cases examined are for pools with concave and convex sidewalls, as shown in Figure 6; this aspect of the sidewall geometry is controlled by the simulation parameter β. The other two cases evaluate effects of pool size at the bottom of the plates via the parameter α. Taken together, the parameters α and β can be adjusted to match a pool shape resulting from the Marangoni effect [1], which is known to influence melt pool shape by causing fluid circulation in the pool to go one way or the other due to liquid surface tension; one case producing a wider more shallow pool while the other producing a deeper more narrow pool.

With respect to β, two cases are demonstrated representing non-constant slope with respect to the plate thickness dimension: 1) curvature of pool is concave, and 2) curvature of pool is convex; these cases are simulated using values for $\beta = 0.25, 0.75$ respectively, while $\alpha = 0.75$ and $||\mathbf{v}_p|| = 15$ are fixed and identical to one case in the weld speed study; microstructures are shown in Figures 12 to 14 – these microstructures can be compared with the case for $||\mathbf{v}_p|| = 15$ in the previous section. The visual affect of β (convex or concave) in the longitudinal section view is not obvious. However, it does affect the width of the strip of smaller equiaxed grains (top view) in the FZ; note that this strip is more narrow for $\beta = 0.25$ than for $\beta = 0.5, 0.75$; the parameter $\alpha = 0.75$ is also a dependent factor.

As a final demonstration on the shape parameters, α is adjusted down to $\alpha = 0.5$ which shrinks the size of the pool at the bottom of the plate; this produces a more obvious effect from β which is also varied as a demonstration. See Figures 15 to 17. When $\beta = 0.0$, curved grains appear in the transverse section view and the longitudinal view has columnar type growth along the centerline in the thickness direction.

4.1.4 Pulsed power demonstration

For comparative purposes, the pulse model is demonstrated using the same model parameters used in the weld speed study; in addition to shape and weld speed parameters given in Table 2, the pulse model parameters used were $A = .25$, and $N = 64$. Recall that A is the fraction of pool size increase and N is the period of pulse power oscillations. The pulse model effect is clearly visible in Figure 18; note that this figure can be directly compared with Figure 9. The period of pulse oscillation produces a spatial frequency that depends upon

weld speed. At the lowest speed, the pulse effect somewhat interrupts the epitaxial growth of very long grains shown in Figure 9 and also produces a more subtle spatial frequency and artifact in the HAZ.

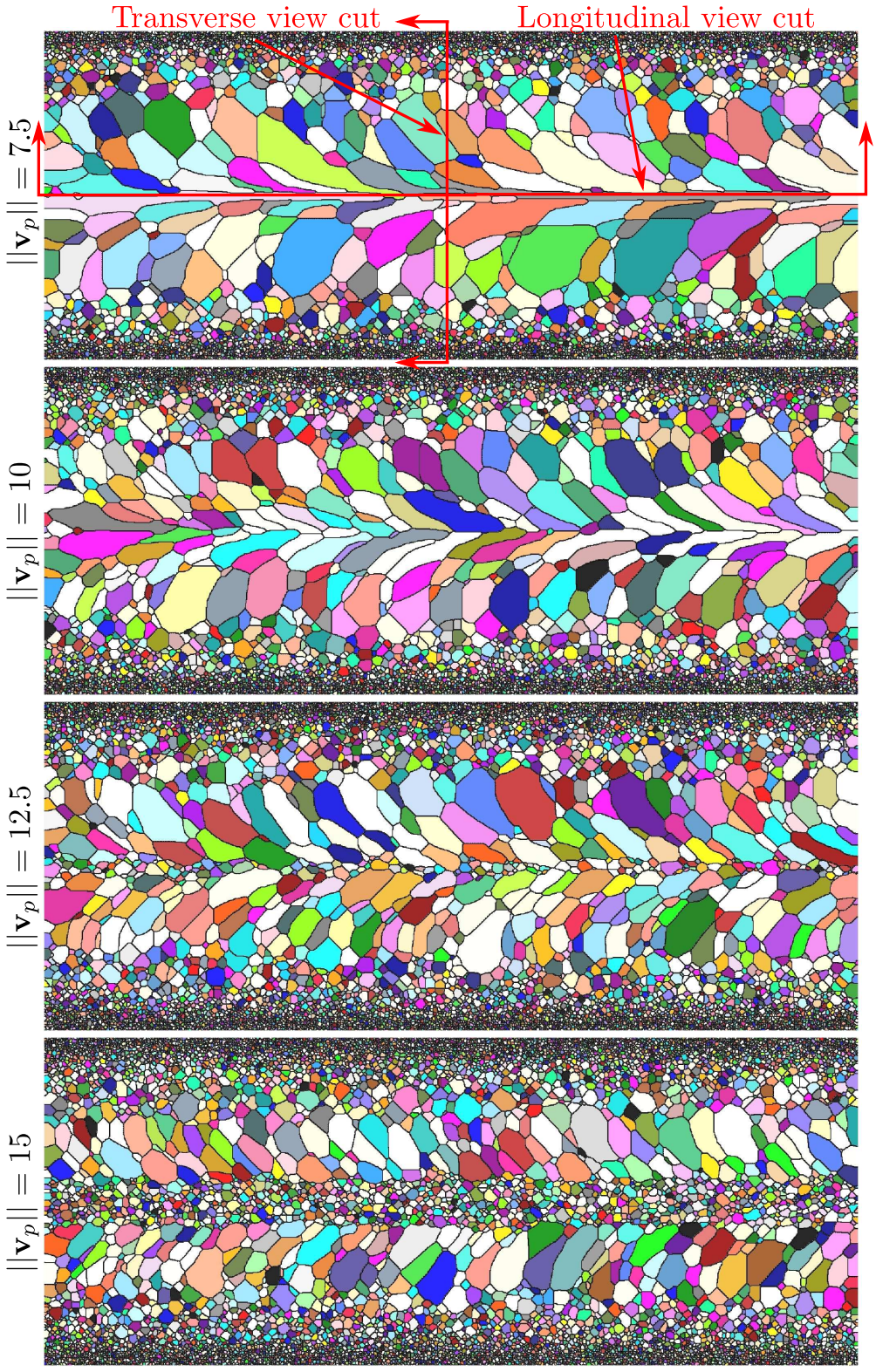

Figure 9: Weld speed study – top view of predicted microstructures; $\alpha = 0.75, \beta = 0.5$; see Table 2 for additional model parameters used. Note indicators in top image for locations of transverse and longitudinal cut views used in subsequent figures.

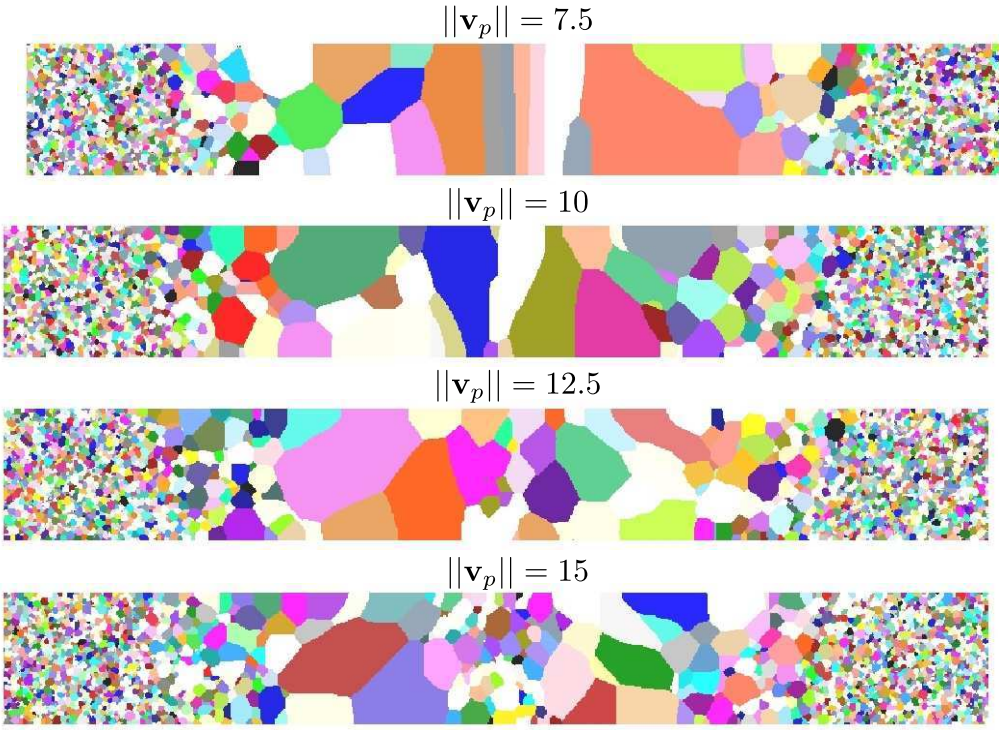

Figure 10: Weld speed study – transverse section view of predicted microstructures; $\alpha = 0.75, \beta = 0.5$; see Table 2 for additional model parameters used.

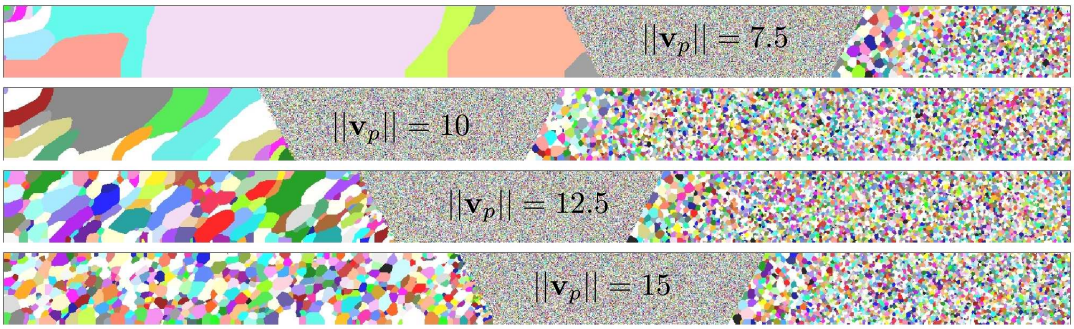

Figure 11: Weld speed study – longitudinal section view (centerline of weld axis) of predicted microstructures; $\alpha = 0.75, \beta = 0.5$; see Table 2 for additional model parameters used. These images depict the shape of the pool and grain growth in front and behind the pool along the centerline (weld axis); the particular location of the pool in each image is not otherwise consequential.

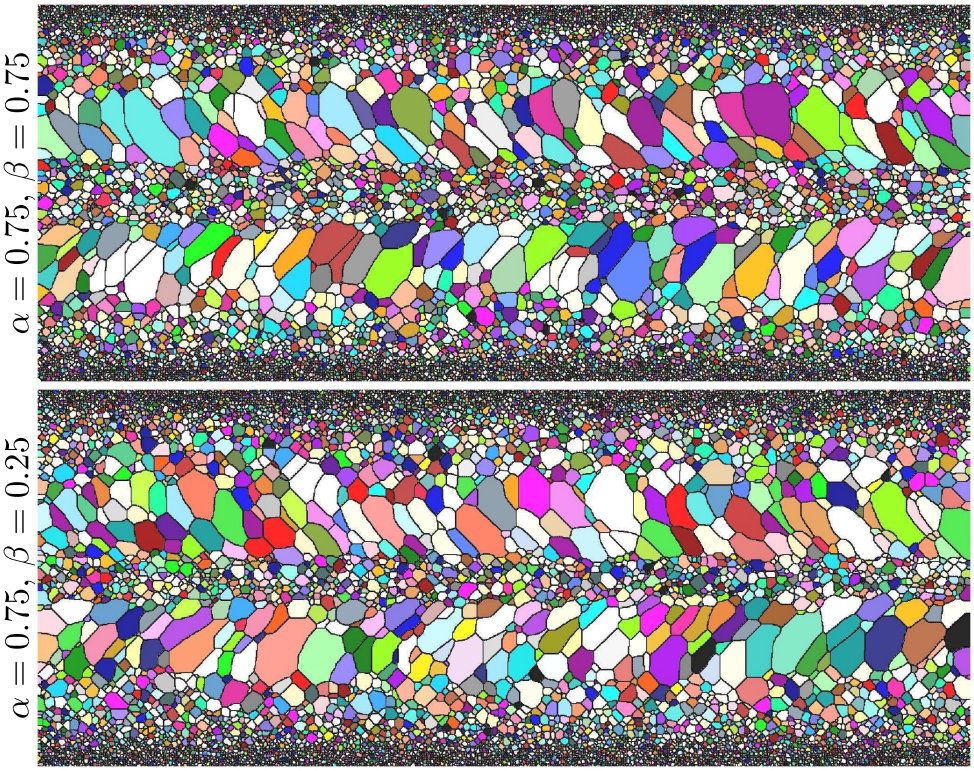

Figure 12: Convexity ($\beta = 0.75$) and concavity ($\beta = 0.25$) study: top view of predicted microstructures with $||\mathbf{v}_p|| = 15.0$; compare Figure 9.

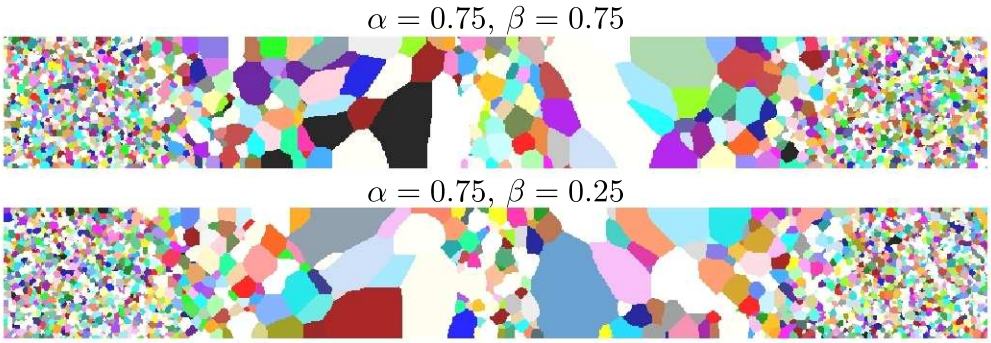

Figure 13: Convexity ($\beta = 0.75$) and concavity ($\beta = 0.25$) study: transverse cut of predicted microstructures with $||\mathbf{v}_p|| = 15.0$; compare Figure 10.

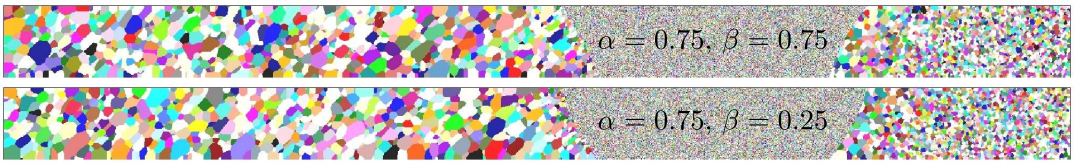

Figure 14: Convexity ($\beta = 0.75$) and concavity ($\beta = 0.25$) study: longitudinal cut of predicted microstructures with $||\mathbf{v}_p|| = 15.0$; compare Figure 11.

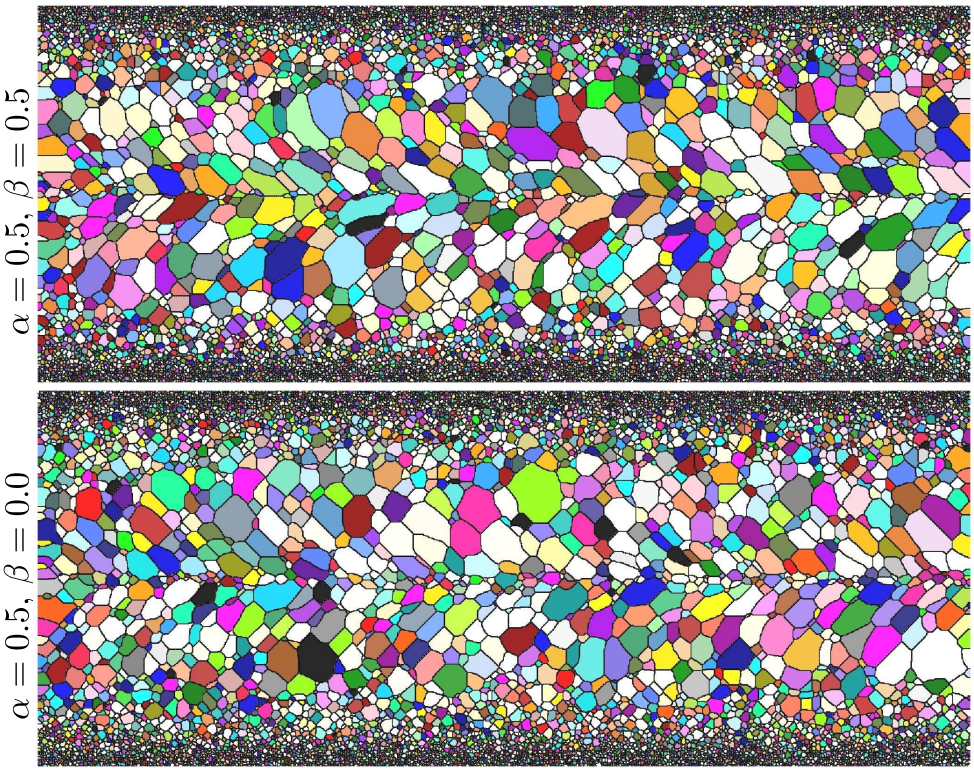

Figure 15: Size and shape study: top view of predicted microstructures with $||\mathbf{v}_p|| = 15.0$.

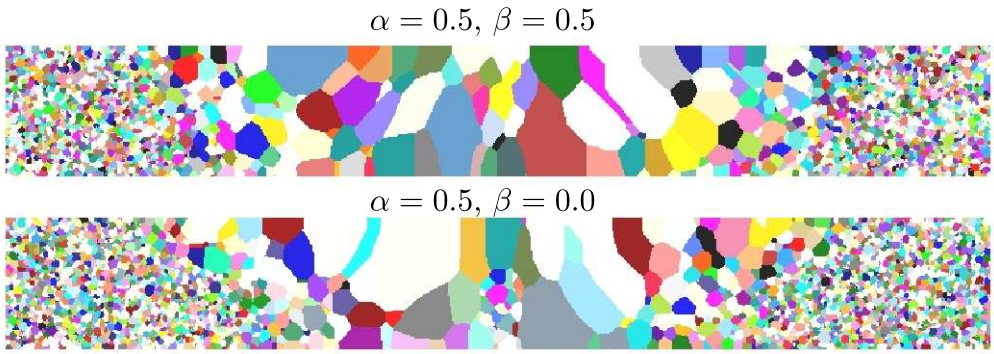

Figure 16: Siza and shape study: transverse cut of predicted microstructures with $||\mathbf{v}_p|| = 15.0$.

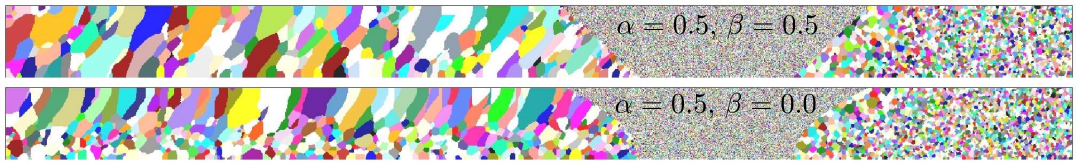

Figure 17: Size and shape study: longitudinal cut of predicted microstructures with $||\mathbf{v}_p|| = 15.0$.

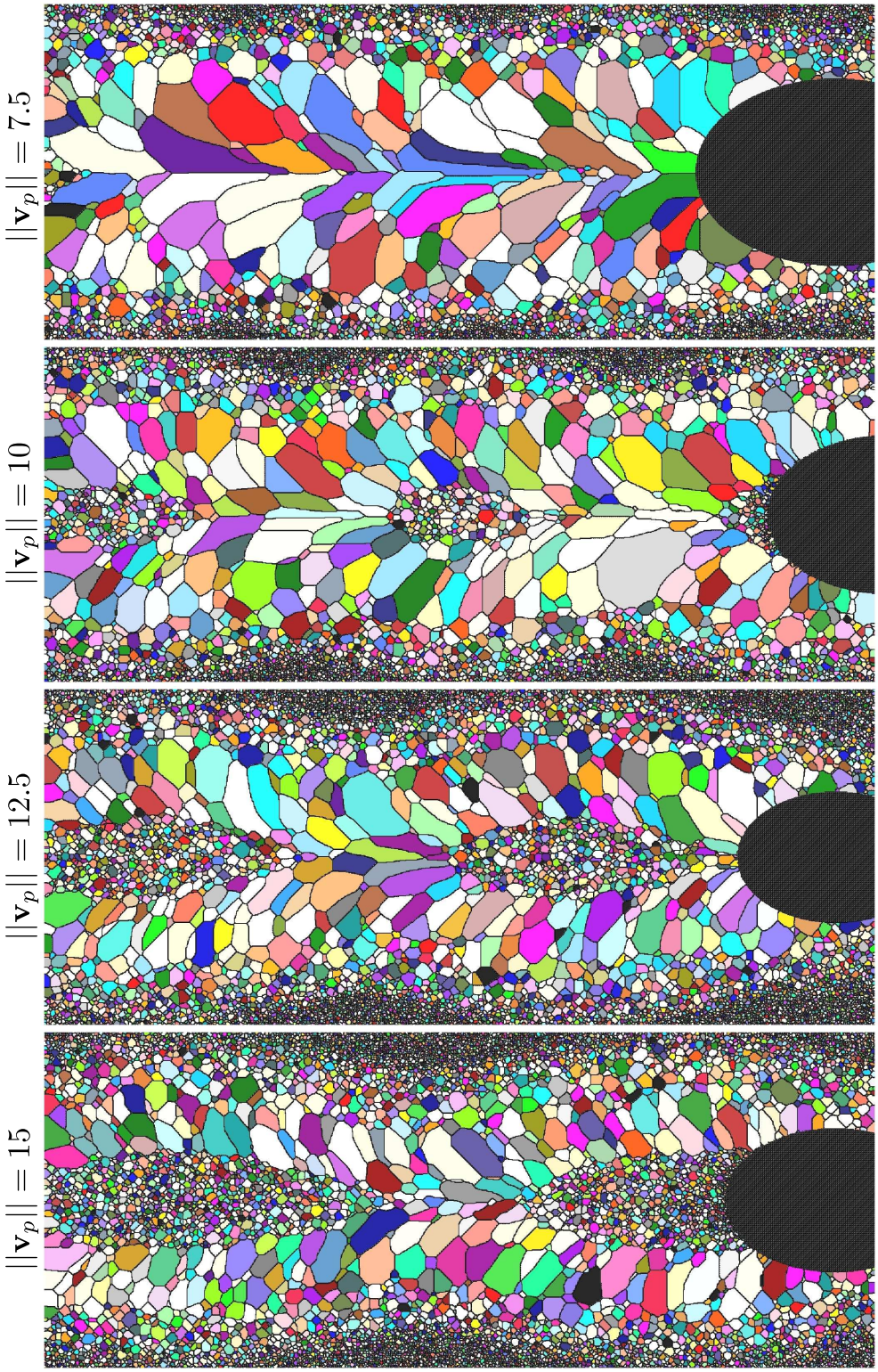

Figure 18: Pulsed weld speed study – top view of predicted microstructures; $\alpha = 0.75, \beta = 0.5$, see Table 2 for remaining model parameters; pulse parameters used are $A = 0.25$, $N = 64$. Weld speeds increase from top to bottom. All parameters being the same except for the addition of pulsed power, compare Figure 9.

5 Summary and conclusions

This report describes and demonstrates a new model for grain growth during welding. The model is implemented in the SPPARKS C++ kinetic Monte Carlo computational framework and can run large scale massively parallel simulations using billions of sites; this resolution is sufficient to enable weld design at welding length scales (measured in millimeters) while simultaneously simulating grain growth and evolution (measured in microns).

The model is parameterized to facilitate weld design via weld speed and shape parameters for the pool and heat affected zone; weld speed is a key weld process parameter; shape parameters describe a wide range of possible pool shapes and heat affected zones facilitating design of many possible weld processes including both convex and concave weld pool shapes; pool shapes can also range from very narrow and deep to very wide and shallow representing different fluid flow conditions within the pool. The model also includes a novel and specialized pulsed power welding feature.

Key elements of the model are listed below.

1. Use of initial microstructure representing base metal
2. Potts model for grain growth specialized for welding including temperature dependent grain boundary mobility
3. Novel mathematical treatment of pool shape and heat affected zone
4. Translation of weld pool
5. Optional pulsed power feature which scales pool geometry as a function of time

The model simulates melting, solidification and microstructural evolution of material in the fusion and heat affected zones; it simulates grain growth using normal curvature driven grain growth with grain boundary mobility that is dependent upon a spatial temperature profile. Demonstration calculations depict grain growth which is spatially heterogeneous including both nucleation and epitaxial dominant grain growth. The model was also applied and demonstrated on a special pulsed power welding process.

References

[1] S. Kou. Fluid flow and solidification in welding: Three decades of fundamental research at University of Wisconsin. *Supplement to the Welding Journal*, 91:287–302, 2012.

[2] Wenda Tan and Yung C. Shin. Analysis of multi-phase interaction and its effects on keyhole dynamics with a multi-physics numerical model. *Journal of Physics D: Application Physics*, 47:345501–345518, 2014.

[3] S.A. David, S.S. Babu, and J.M. Vitek. Welding: Solidification and microstructure. *Journal of Materials*, 55(6):14–20, June 2003.

[4] A. Paul and T. Debroy. Free surface flow and heat transfer in conduction mode laser welding. *Metallurgical Transactions B*, 19B:851–858, 1988.

[5] Wenda Tan, Shaoyi Wen, Neil Bailey, and Yung C. Shin. Multiscale modeling of transport phenomena and dendritic growth in laser cladding processes. *Metallurgical Transactions B.*, 42B:1306–1317, 2011.

[6] R. Han, S. Lu, W. Dong, D. Li, and Y. Li. The morphological evolution of the axial structure and the curved columnar grain in the weld. *Journal of Crystal Growth*, 431:49–59, 2015.

[7] W. Tan and Y.C. Shin. Multi-scale modeling of solidification and microstructure development in laser keyhole welding process for austenitic stainless steel. *Computational Materials Science*, 98:446–458, 2015.

[8] Wenda Tan, Neil S. Bailey, and Yung C. Shin. A novel integrated model combining cellular automata and phase field methods for microstructure evolution during solidification of multi-component and multi-phase alloys. *Computational Materials Science*, 50:2573–2585, 2011.

[9] X.H. Zhan, Z.B. Dong, Y.H. Wei, and R. Ma. Simulation of grain morphologies and competitive growth in weld pool of NiCr alloy. *Journal of Crystal Growth*, 311:4778–4783, 2009.

[10] W.J. Zheng, Z.B. Dong, Y.H. Wei, K.J. Song, J.L. Guo, and Y. Wang. Phase field investigation of dendrite growth in the welding pool of aluminum alloy 2A14 under transient conditions. *Computational Materials Science*, 82:525–530, 2014.

[11] Vitaliy Pavlyk and Ulrich Dilthey. Simulation of weld solidification microstructure and its coupling to the macroscopic heat and fluid flow modeling. *Modeling and Simulation in Material Science and Engineering*, 12:S33–S45, 2004.

[12] H.B. Dong and P.D. Lee. Simulation of the columnar-to-equiaxed transition in directionally solidified Al–Cu alloys. *Acta Materialia*, 53:659–668, 2005.

[13] T. Kosekia, H. Inoue, Y. Fukuda, and A. Nogami. Numerical simulation of equiaxed grain formation in weld solidification. *Science and Technology of Advanced Materials*, 4:183–195, 2003.

[14] D. Montiel, L. Liu, L. Xiao, Y. Zhou, and N. Provatas. Microstructure analysis of AZ31 magnesium alloy welds using phase-field models. *Acta Materialia*, 60:5925–5932, 2012.

[15] Shijia Chen, Gildas Guillemot, and Charles-Andre Gandin. 3D Coupled Cellular Automaton (CA)Finite Element (FE) Modeling for Solidification Grain Structures in Gas Tungsten Arc Welding (GTAW). *ISIJ International*, 54:401–407, 2014.

[16] S. Sista, Z. Yang, and T. Debroy. Three-dimensional monte carlo simulation of grain growth in the heat-affected zone of a 2.25Cr-1Mo steel weld. *Metallurgical Transactions B., Process Metallurgy and Materials Processing*, 31:529–536, 2000.

[17] S. Mishra and T. Debroy. Measurements and Monte Carlo simulation of grain growth in the heat-affected zone of Ti6Al4V welds. *Acta Materialia*, 52:1183–1192, 2004.

[18] S. Mishra and T. Debroy. Grain topology in Ti6Al4V welds–Monte Carlo simulation and experiments. *Journal of Physics D: Applied Physics*, 37:2191–2196, 2004.

[19] W.B. Dress, T. Zacharia, and R. Radhakrishnan. Cellular automata modeling of weld solidification structure. December 1993. International Conference on Modeling and Control of Joining Processes, Orlando, Florida.

[20] T. Zacharia, J.M. Vitek, J.A. Goldak, T.A. Debroy, and M. Rappaz H.K.D.H. Bhadeshia. Modeling of fundamental phenomena in welds. *Modeling and Simulation in Materials Science and Engineering*, 3:265–288, March 1995.

[21] M.P. Anderson, D.J. Srolovitz, G.S. Grest, and P.S. Sahni. Computer simulation of grain growth – i. kinetics. *Acta Metallurgica*, 32(5):783–791, 1984.

[22] E.A. Holm and C.C. Battaile. The computer simulation of microstructural evolution. *Journal of the Minerals Metals and Materials Society*, 53:20–23, 2001.

[23] A. Garcia, V. Tikare, and E. Holm. Three-dimensional simulation of grain growth in a thermal gradient with non-uniform grain boundary mobility. *Scripta Materialia*, 59:661–664, 2008.

[24] Steve Plimpton, Corbet Battaile, Mike Chandross, Liz Holm, Veena Tikare, Greg Wagner, Ed Webb, and Xiaowang Zhou. Crossing the mesoscale no-man's land via parallel kinetic monte carlo. Technical Report SAND2009-6226, Sandia National Laboratories, October 2009.

[25] T.M. Rodgers, J.D. Madison, V. Tikare, and M.C. Maguire. Predicting mesoscale

microstructural evolution in electron beam welding. *JOM: The Journal of The Minerals, Metals & Materials Society*, 68(5):1419–1426, May 2016.

[26] Steve Plimpton, Aidan Thompson, and Alex Slepoy. *SPPARKS*, 2016. http://spparks.sandia.gov.

[27] Alexander Konyukhov and Karl Schweizerhof. *Computational Contact Mechanics*. Springer, 2013.

[28] Les Piegl and Wayne Tiller. *The NURBS Book*. Springer, second edition, 1997.

DISTRIBUTION:

1	MS 1320	John A. Mitchell, 01444
1	MS 1320	Veena Tikare, 01444
1	MS 0899	Technical Library, 09536


Sandia National Laboratories